

## Threshold behavior of local gradient Richardson number in strongly stratified nonequilibrium turbulence

Qi Zhou <sup>\*</sup>

Department of Civil Engineering, University of Calgary, 2500 University Drive NW, Calgary, Alberta, Canada T2N 1N4



(Received 17 July 2022; accepted 5 October 2022; published 20 October 2022)

In this paper we examine the possible self-organization of strongly stratified turbulence around a local critical state by analyzing a dataset of a numerically simulated stratified turbulent wake. To facilitate the analysis, the turbulent flow field is decomposed into a “large-scale” flow of horizontal scales greater than the Ozmidov scale,  $\ell_O$ , and a “small-scale” flow of scales below  $\ell_O$ . A local gradient Richardson number,  $Ri$ , characterizing the large-scale flow is calculated and then utilized to produce conditional sampling of various turbulence statistics relevant to the local dynamics. While the bulk turbulence is observed to decay by approximately one order of magnitude in terms of the dissipation rate, the median  $Ri$  has remained nearly constant due to the self-organization of flow structures under strong stratification; the subsampled  $Ri$  distribution peaks around  $1/4$  for regions in the upper quartile of local dissipation. Regions of small  $Ri$  are found to be associated with large dissipation and large net transfer of energy to the small scales. Regions of “back-scatter” of kinetic energy to large scales, where the local eddy viscosity,  $\nu_e$ , takes a negative value, are also observed. Occurrence of a large magnitude of both positive and negative  $\nu_e$  appears to be most frequent around the critical value of  $Ri \sim 1/4$ , indicating an intense two-way exchange of kinetic energy between the large and small scales around the local critical state. The threshold behavior of  $Ri$  underscores the dynamical significance of the critical  $Ri$  of  $1/4$  for locally self-sustained turbulence in a strongly stratified configuration and bears some resemblance to the celebrated self-organized criticality dynamics [Bak *et al.*, *Phys. Rev. Lett.* **59**, 381 (1987)].

DOI: [10.1103/PhysRevFluids.7.104802](https://doi.org/10.1103/PhysRevFluids.7.104802)

### I. INTRODUCTION

The hypothesis of self-organized criticality [1,2] was introduced to the investigation of turbulent flows in a stably stratified fluid recently [3,4] and was used to construct reduced models for strongly stratified turbulence [5]. The concept of self-organized criticality (SOC) was employed to characterize the interplay between the stable density stratification and the vertical shear of horizontal mean velocity. It is hypothesized that the flow self-organizes into a quasiequilibrium or critical state around which the SOC-like dynamics take place in a cyclic way. Such a self-regulated state is characterized by a critical value of a gradient Richardson number of approximately  $1/4$ , i.e.,  $Ri \sim 1/4$ , a condition that resembles the well-known Miles-Howard criterion based on the classical linear stability analysis of parallel inviscid steady shear flows [6,7]. Alternative interpretations of this critical state, for which Ref. [3] provided an extensive review, include a constant-flux layer near a boundary following the Monin-Obukhov similarity theory (see, e.g., Refs. [8,9]), as well as a state of cyclic or marginal instability due to the effects of external forcing (see, e.g., Refs. [10–13]).

---

\*qi.zhou1@ucalgary.ca

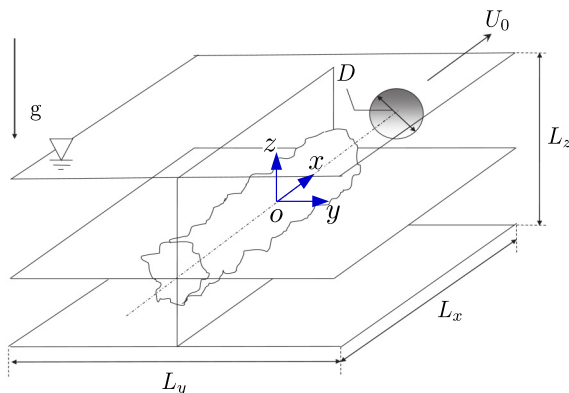


FIG. 1. Computational domain (not drawn to scale) for simulating a temporally evolving, stably stratified towed-sphere wake [22,26]. The sphere of diameter  $D$  is assumed to be towed along the  $x$  axis at speed  $U_0$  such that the centerline of the wake is at  $(y, z) = (0, 0)$ . The origin  $(x, y, z) = (0, 0, 0)$  is at the center of the domain. The domain is of dimensions  $L_x \times L_y \times L_z = (56/3)D \times (28/3)D \times (20/3)D$  and is resolved by  $N_x \times N_y \times N_z = 1024 \times 512 \times 609$  grid points.

According to Ref. [4], the SOC-like dynamics in stratified geophysical turbulence satisfy two criteria, which are paraphrased as follows:

- (1) Turbulence is attracted to the critical state of  $Ri \sim 1/4$  through self-organization.
- (2) Characteristic length scale of intermittent events that maintain SOC follows a power-law distribution to reach a scale-invariant state [14].

Although the notion of SOC is shared by Refs. [3,4], these two pioneering studies had some considerable differences. Salehipour *et al.* [3], using numerical simulations, considered the turbulence ensuing the breakdown of Holmboe wave instability (HWI) at a sharp density interface—no external forcing is applied to maintain the turbulence, while the background vertical shear is introduced as an initial condition. The self-maintenance of SOC is through the “scouring” motions driven by counterrotating vortex pairs that are intrinsic to Holmboe waves within which turbulence is embedded. Although the HWI-induced turbulence decays weakly with time (see Fig. 1 of Ref. [3]), a quasiequilibrium is reached, internally and spontaneously, between the shear production, viscous dissipation, and scalar mixing. It is also suggested that Kelvin-Helmholtz instability (KHI) may not initiate SOC turbulence because of the mismatch of  $Ri$  with the critical value of  $1/4$  (see their Fig. 13). Smyth *et al.* [4], on the other hand, focused on field measurements of the equatorial undercurrent and hypothesized a clear-cut separation of a growth regime and a decaying regime by  $Ri \sim 1/4$  at various phases of the well-defined SOC cycle (see their Fig. 3). In this context, the maintenance of the quasiequilibrium state, one that is characterized by  $Ri \sim 1/4$ , relies critically on two ingredients: an external forcing (i.e., an easterly trade wind) that injects energy to the mean flow, and the resulting normal-mode instability that grows and leads to intense turbulent diffusion when  $Ri < 1/4$  (presumably this instability is analogous to KHI which are commonly seen in oceanic measurements; see, e.g., Ref. [15–18]). The fact that  $Ri$  fluctuates around  $1/4$  is also considered a hallmark of the marginal instability (MI) within certain oceanic flows and has been utilized to examine the mixing properties associated with them [19,20].

In this paper, we aim to explore stratified turbulence dynamics that potentially resemble SOC or MI in a considerably different flow scenario: turbulence in a decaying free-shear stratified flow represented by a towed-sphere wake in a uniformly stratified fluid. The central objective of the paper is to identify elements of SOC or MI dynamics within this particular flow: Specifically, is there evidence that the threshold behavior of  $Ri$ , i.e., that  $Ri$  fluctuates around a critical value, also exists in turbulence that undergoes significant decay (i.e., no equilibrium can be reached overall) due to the

combined effects of strong stratification and the absence of external forcing [4]? And, if so, what is the maintenance mechanism for the local and internal quasiequilibrium within the turbulence, much like what is observed in Ref. [3], but without Holmboe waves acting as the specific internal driving force? We aim to clarify if SOC-like dynamics can be achieved only through a specific external forcing [4] or a specific type of primary instability [3], both of which are absent in the flow under consideration; in other words, can the self-organization around some critical state emerge locally and spontaneously in preexisting turbulence in a strongly stratified shear flow that is intrinsically out of equilibrium?

Stratified wake turbulence, as it decays in time, undergoes a distinct life cycle [21] in which the effects of stratification become increasingly dominant on the large-scale motions and the turbulence activity becomes increasingly intermittent [22–25]. The identification of SOC-like dynamics would, therefore, require a methodology that takes into account the potential coexistence of subcritical, critical, and supercritical dynamics simultaneously in the flow. The bulk of this analysis will thus be conducted using a locally defined gradient Richardson number,  $Ri$ , upon which conditional statistics are constructed in order to reveal any threshold behavior of  $Ri$  and its implications for the local dynamics. The statistics are based on a numerical dataset consisting of various snapshots taken from an early-to-intermediate stratified wake, as well as a filter-based flow decomposition technique that separates the mean flow and turbulence in a way that is appropriate for our analysis. The dataset will be introduced in Secs. II A and II B, and the flow decomposition that enables the locally defined  $Ri$  and various other turbulence statistics will be introduced in Sec. II C. In Sec. III conditional sampling of various turbulence statistics relevant to the SOC-like dynamics will be presented, in an attempt to interpret the dynamical significance of  $Ri$  and the potential maintenance mechanism of stratified turbulence. We conclude in Sec. IV with a summary of the key findings and recommendations for future work.

## II. METHODOLOGY

### A. Numerical simulation

In this paper, we consider a temporally evolving stratified towed-sphere wake (Fig. 1) of wake Reynolds number  $Re \equiv U_0 D / \nu$  of 25 000 and internal Froude number  $Fr = 2U_0 / ND$  of 4. Here  $U_0$  is the tow speed,  $D$  is the sphere diameter,  $N$  is the buoyancy frequency (which is a constant in space), and  $\nu$  is the kinematic viscosity. The Prandtl (or Schmidt) number is set to be unity in this simulation. The wake simulation is initialized using a two-stage auxiliary presimulation that accounts for the effects of the sphere [22]. The top surface of the domain is free-slip and the bottom is no-slip, mimicking a typical laboratory flume. Wave-absorbing sponge layers are configured around the domain to damp out any internal gravity waves emitted by the turbulence and reflected off the top and bottom boundaries, so that the waves do not reenter the domain to contaminate the turbulence. The pseudospectral Navier-Stokes solver used to generate the specific dataset employs Fourier discretization in the horizontal directions ( $x$  and  $y$ ) and Legendre-polynomial-based subdomain discretization in the vertical direction ( $z$ ). For a compact review of the numerical scheme originally developed by Diamessis *et al.* [26] to solve the incompressible Navier–Stokes equation under Boussinesq approximation, the readers are referred to Sec. III of a recent paper, Ref. [24].

The particular Navier-Stokes solver [26] employed here has been implemented extensively to investigate large-scale characteristics of the turbulence [23,24,27] and internal waves emitted by a wake [23,28,29]. Spectral filtering and a penalty scheme at the subdomain interfaces (in  $z$ ) were implemented to ensure numerical stability in the aforementioned studies. For adequate resolution of small-scale turbulence, the grid resolution in the present study (see the caption of Fig. 1) has been chosen such that the grid spacing in the horizontal directions,  $h$ , is no more than 3.81 times the Kolmogorov scale,  $\ell_K$ ; such a ratio of  $h/\ell_K$  (Table I) is comparable to similar direct simulations of stratified shear flows found in the literature [30–32]; the vertical grid points are concentrated near the wake centerline for enhanced resolution of the turbulence, e.g., the average grid spacing

TABLE I. Nondimensional parameters of numerical dataset of a stratified wake of  $Re = 25\,000$  and  $Fr = 4$ . Four snapshots (or cases) at various dimensionless time,  $Nt$ , are considered, where  $t$  is the time elapsed since the passage of the sphere. The ratio  $h/\ell_K$  is a measure of horizontal grid resolution discussed in Sec. II A;  $Re_b$  and  $Fr_h$  characterize the properties of stratified turbulence considered in Sec. II B;  $L_H/D$  and  $L_V/D$  are measures of mean wake dimensions as defined in Sec. II B.

Case	$Nt$	$Re_b$	$Fr_h$	$h/\ell_K$	$L_H/D$	$L_V/D$
A	2.0	19	0.030	3.81	0.406	0.396
B	6.0	9.4	0.020	3.21	0.464	0.376
C	10.0	4.3	0.015	2.64	0.484	0.378
D	19.0	1.5	0.0084	2.03	0.529	0.370

for  $z/D \in [-1, 1]$  is approximately three times finer than the horizontal grid spacing. Spectral filtering is relaxed substantially as compared to previously reported runs (e.g., Ref. [24]) using the same solver for investigating large-scale characteristics of wake turbulence. The filtering is used minimally only to a degree that is needed to contain the inevitable round-off and aliasing errors (see, e.g., Ref. [33]); the weak filtering applied here, which impacts the wave numbers above the 78th percentile in terms of their magnitude, is comparable to the dealiasing operation that is commonly used in pseudospectral simulations (see, e.g., Refs. [30,34,35]). The penalty scheme [26] applied to the subdomain interfaces is turned off as this treatment becomes redundant in a well-resolved simulation. The simulation was carried out using 256 parallel processors provided by Compute Canada's Cedar cluster, costing approximately 184 000 core hours to complete.

### B. Mean flow and turbulence characteristics

The analysis to be presented is mainly focused on four time instances (i.e., four cases) in the wake's evolution, which are summarized in Table I. As shown in Fig. 1, the spatial extent of the wake turbulence is finite in both span ( $y$ ) and vertical ( $z$ ) directions. It is therefore of interest to define the exact width and height of the flow. We follow the approach used in Ref. [24] to define the core region of the wake for which statistics are taken. First, the velocity field  $\mathbf{U}(\mathbf{x}, t) \equiv (U, V, W)$  can be decomposed into a mean flow in the  $x$  direction and the fluctuation velocity field (denoted by a superscript  $'$ ):

$$\mathbf{U}(\mathbf{x}, t) = (\langle U \rangle_x, 0, 0) + (U', V', W'). \quad (1)$$

Here and elsewhere,  $\langle \cdot \rangle_x$  denotes an average in the statistically homogeneous  $x$  direction, and  $\mathbf{U}' \equiv (U', V', W')$  is fluctuation velocity. (Note that the streamwise direction  $x$  is periodic and homogeneous, as a result of the classic approach [36] to simulate a spatially evolving shear flow as a temporally evolving one.) The  $x$ -averaged mean flow  $\langle U \rangle_x$  is then fit to a two-dimensional Gaussian profile,

$$\langle U \rangle_x(y, z, t) = U_c(t) \exp \left[ -\frac{1}{2} \left( \frac{y}{L_H(t)} \right)^2 - \frac{1}{2} \left( \frac{z}{L_V(t)} \right)^2 \right],$$

where  $U_c$  is the mean centerline velocity, and  $L_H$  and  $L_V$  are the characteristic mean wake width and height, respectively. The  $L_H/D$  and  $L_V/D$  values are tabulated in Table I for all four cases. It can be seen that  $L_H$  has grown considerably during the time interval of interest,  $2.0 \leq Nt \leq 19.0$ , while  $L_V$  fluctuates weakly within a narrow range of values, following the collapse of the wake due to stratification [21].

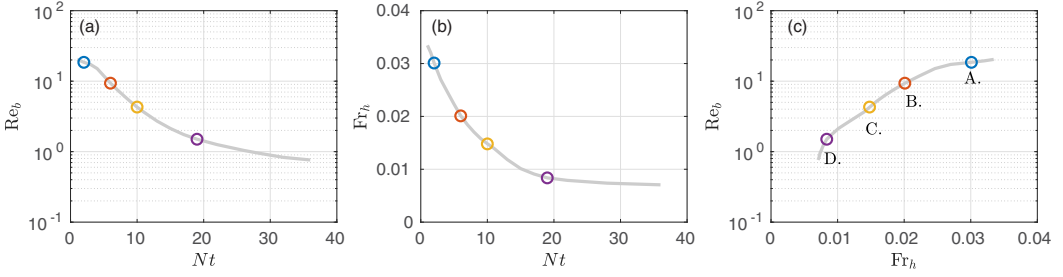


FIG. 2. Characteristics of stratified turbulence in the stratified wake under consideration. (a) Time series of the buoyancy Reynolds number,  $Re_b$ , (b) time series of the horizontal turbulent Froude number,  $Fr_h$ , and (c)  $Re_b$  plotted against  $Fr_h$ . Circles drawn in various colors correspond to the cases tabulated in Table I and labeled in panel (c).

Following the definition of the wake's dimensions, the wake's core region is then defined [24] as a volume of the shape of an elliptic cylinder centered around  $(y, z) = (0, 0)$  (see Fig. 1), where

$$\frac{y^2}{(2L_H)^2} + \frac{z^2}{(2L_V)^2} \leq 1. \quad (2)$$

In the remainder of the paper, we will use  $\langle \cdot \rangle$  to denote a volume average over the wake's core region as defined above. For example, the mean dissipation rate of turbulent kinetic energy (or simply dissipation) within the wake core can be estimated as  $\langle \varepsilon \rangle$ , where

$$\varepsilon(\mathbf{x}, t) \equiv 2\nu S'_{ij} S'_{ij} \quad (3)$$

is the locally defined dissipation rate determined by the rate of strain tensor  $S'_{ij} \equiv (1/2)(\partial U'_i/\partial x_j + \partial U'_j/\partial x_i)$  due to the fluctuation velocity,  $\mathbf{U}'$ . Two length scales can be defined using the volume-averaged dissipation,  $\langle \varepsilon \rangle$ :

$$\ell_K \equiv \left( \frac{\nu^3}{\langle \varepsilon \rangle} \right)^{1/4} \quad \text{and} \quad \ell_O \equiv \left( \frac{\langle \varepsilon \rangle}{N^3} \right)^{1/2},$$

where  $\ell_K$  is the Kolmogorov scale, characterizing the smallest dissipative-scale eddies, and  $\ell_O$  is the Ozmidov scale, characterizing the largest horizontal scale that can overturn (e.g., Ref. [37]) or the cut-off scale below which isotropic three-dimensional turbulence could exist (e.g., Ref. [38]); we will revisit  $\ell_O$  in the next subsection.

A first appreciation of the time evolution of stratified turbulence characteristics can be obtained from Fig. 2—that the turbulence under consideration is nonequilibrium and strongly stratified. Two dimensionless parameters, the buoyancy Reynolds number,  $Re_b$ , and the horizontal turbulent Froude number,  $Fr_h$ , are plotted against the dimensionless time,  $Nt$ , for the four cases tabulated in Table I.  $Re_b$  and  $Fr_h$  are defined as

$$Re_b \equiv \frac{\langle \varepsilon \rangle}{\nu N^2} \quad \text{and} \quad Fr_h \equiv \frac{\sqrt{\langle U'^2 + V'^2 \rangle}}{N \ell_h},$$

respectively, where  $\ell_h$  is the horizontal integral scale of turbulence, which is calculated using the streamwise spectrum of  $U'$  (see details in Appendix C of Ref. [24]). The magnitude of  $Re_b$  measures the separation between the Ozmidov and Kolmogorov scales,  $\ell_O/\ell_K \sim Re_b^{3/4}$  [37], and  $Fr_h$  is a key indicator of the degree of stratification and anisotropy that is commonly used in scaling analysis of strongly stratified flows (e.g., [39–41]).

As can be seen in Fig. 2(a), the wake turbulence undergoes significant decay during the time period under examination,  $2.0 \leq Nt \leq 19.0$ , as the value of  $Re_b$  decays by about one order of magnitude from 19 to 1.5. This observation is different from the HWI case considered in Ref. [3],

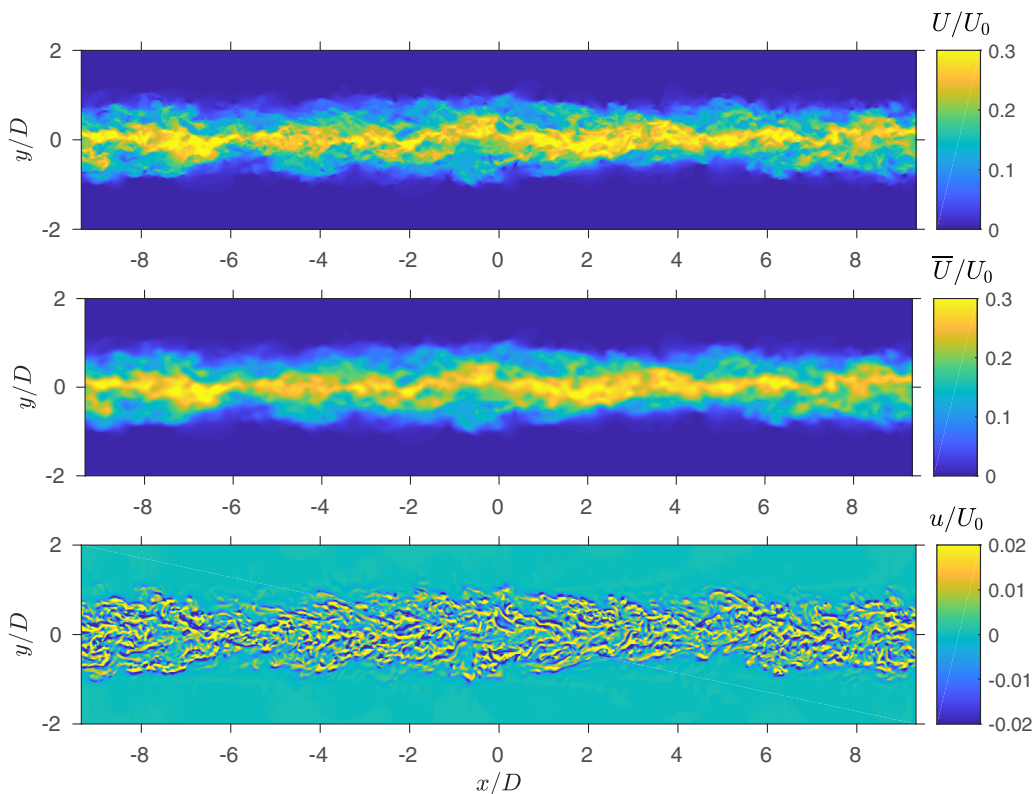


FIG. 3. Decomposition of the streamwise velocity,  $U = \bar{U} + u$ , visualized over the  $oxy$  horizontal transect taken at  $z = 0$  (Fig. 1) for case A ( $Nt = 2.0$ ). Top, middle, and bottom panels correspond to  $U$ ,  $\bar{U}$ , and  $u$ , respectively. Velocities are normalized by the tow speed,  $U_0$ . The images are close-up views for a width of  $4D$  along the wake centerline at  $y = 0$ ; the computational domain is  $7/3$  times wider (see Fig. 1) than what is shown in this figure.

where a global quasiequilibrium is reached in terms of the energetics (see their Fig. 3), and it is different from the oceanic case considered in Ref. [4], where the turbulent kinetic energy can grow in certain phases of the dynamical cycle. In the specific context of a stratified wake, Spedding [21] defined a nonequilibrium (NEQ) regime for  $2 \leq Nt \leq 50$ , a regime that overlaps with the cases under consideration in this paper.

Figure 2(b) shows that  $Fr_h$  also decays in time, indicating a stronger influence of stratification on the turbulence as the flow evolves. As can be seen in Fig. 2(c), out of the four cases considered in this paper, cases B, C, and D actually satisfy the conditions of  $Re_b \geq 1$  and  $Fr_h \leq 0.02$  which were used in Ref. [24] to define the strongly stratified regime [41] [a regime that is also termed the layered anisotropic stratified turbulence regime (LAST) in other references, e.g., [42,43]] for the context of wake turbulence. [Incidentally, this regime has not been as extensively studied by numerical simulations as the weakly stratified turbulence regime—e.g., see Fig. 1(b) of Ref. [5]—presumably due to the considerable computational cost associated with the LAST regime.] Within this regime, stratification has strong effects on the horizontal integral-scale eddies, as indicated by  $Fr_h \ll 1$ ; strong stratification drives the spontaneous formation of the layered anisotropic flow structure in the wake [24], which is an essential characteristic of this regime. At the same time, there still exists a dynamic range of scales between  $\ell_O$  and  $\ell_K$  which allows for small-scale turbulence [44] while  $Re_b \geq 1$ .

### C. Flow decomposition and filtering

The common definitions of gradient Richardson number,  $Ri$ , typically include an averaging procedure on the velocity gradients, either in space [3] or in time [4], such that the resulting  $Ri$  is, by nature, a descriptor of the mean flow for its potential for triggering turbulence. It is postulated in Sec. I that the SOC-like dynamics in stratified wake turbulence, if they exist, would occur in a local and transient way, while globally the bulk turbulence undergoes significant decay (Fig. 2). It follows from this postulation that subcritical ( $Ri > 1/4$ ), critical ( $Ri = 1/4$ ), and supercritical ( $Ri < 1/4$ ) regions could coexist in the flow simultaneously. Quasiequilibrium can be achieved locally by a cyclic exchange of energy between the mean flow and the turbulence, the definition of which seems most appropriate when formulated in a local sense. It is thus important to construct a version of  $Ri$  that is appropriate for describing the large-scale dynamics that could vary in space. With this locally defined  $Ri$ , one can then perform conditional sampling of various quantities that are relevant to the local dynamics.

The critical step towards a local  $Ri$  is to separate the mean flow from the turbulence, or rather to decompose the flow field into large scales that could drive local shear instabilities, and small scales that are not directly impacted by stratification. It is therefore of benefit to consider a cut-off length scale above which is the large scale or mean flow, and below which is the small scale or turbulence—in our context, the natural choice for this cut-off scale is the Ozmidov scale,  $\ell_o$ , which is the largest horizontal scale that possesses enough kinetic energy to overcome the potential energy barrier needed to overturn [45] and can be considered as the transition scale between stratified turbulence and classical three-dimensional turbulence [37]. We thus assume that  $\ell_o$  characterizes the largest eddies that are not directly impacted by stratification: Scales smaller than  $\ell_o$  can overturn and exhibit behaviors similar to isotropic turbulence—eddies smaller than or of order  $\ell_o$  are hardly distorted by stratification and share many characteristics with isotropic turbulence; scales larger than  $\ell_o$  are manifestly affected by stratification and subject to possible self-organization which we attempt to identify by characterizing those large-scale flows. It is worth noting that the use of  $\ell_o$  as an order-of-magnitude approximation for the cut-off scale between the isotropic and anisotropic dynamics is based merely on scaling arguments; testing quantitatively whether  $\ell_o$  is precisely such a cut-off is outside the scope of the current study.

Indeed, a filter-based scheme is implemented to postprocess the numerical dataset so that horizontal scales above and below  $\ell_o$  can be separated. The postprocessing filter decomposes the flow into a large-scale flow component,  $\overline{\mathbf{U}}(\mathbf{x}, t) \equiv (\overline{U}, \overline{V}, \overline{W})$ , and a residual small-scale flow component,  $\mathbf{u}(\mathbf{x}, t) \equiv (u, v, w)$ . The filter-based decomposition reads

$$\mathbf{U}(\mathbf{x}, t) = (\overline{U}, \overline{V}, \overline{W}) + (u, v, w), \quad (4)$$

where all velocity components shown on the right-hand side vary in both space (all three directions) and time, and the overline denotes the filter operation. Figure 3 shows an example of the decomposition for the  $U$  velocity in case A. The filtering is performed over horizontal transects of all three velocity components using a two-dimensional low-pass Gaussian filter (see, e.g., Ref. [46]) with  $\ell_o$  specified as the standard deviation of the filter function. The large-scale gradient Richardson number,  $Ri(\mathbf{x}, t)$ , can then be calculated using the filtered velocity,

$$Ri \equiv \frac{N^2}{\left(\frac{\partial \overline{U}}{\partial z}\right)^2 + \left(\frac{\partial \overline{V}}{\partial z}\right)^2} = \frac{N^2}{S^2}, \quad (5)$$

which we will revisit in Sec. III A. Visual inspection of the density field suggests that density fluctuations due to wake turbulence generate vertical density gradients that are considerably weaker than the background density gradient characterized by  $N^2$ , presumably due to the strong stratification prescribed for this flow. Therefore, we opt to use the background buoyancy frequency  $N$  (which is a constant) in the above definition of  $Ri$  as a descriptor of the large-scale or mean density gradient.

In addition to  $Ri$  itself, we will also examine the exchange of energy between the large (filtered) and small (residual) scales in Secs. III C and III D. The formulation for this analysis can often be

found in the literature of large-eddy simulations (LES), e.g., Sec. 13 of Ref. [47], and here a brief review is provided. Again, our aim in this paper is not to formulate an LES for the flow, but to use the formulation as a diagnostic tool for analyzing the data.

Analogous to the Reynolds stress tensor in Reynolds-averaged Navier-Stokes equation, a residual-stress tensor appears in the filtered momentum equation and is defined as

$$\tau_{ij}^R \equiv \overline{U_i U_j} - \overline{U_i} \overline{U_j}.$$

The residual kinetic energy,  $k_r$ , is half of the trace of  $\tau_{ij}^R$ ,  $k_r \equiv \tau_{ii}^R/2$ , and the anisotropic residual-stress tensor,  $\tau_{ij}^r$ , can be written as

$$\tau_{ij}^r \equiv \tau_{ij}^R - \frac{2}{3} k_r \delta_{ij}, \quad (6)$$

where  $\delta_{ij}$  is the Kronecker delta. A sink term,  $\mathcal{P}_r$ , appears in the energy budget for the filtered velocity field (see Sec. 13.3.3 of Ref. [47]), which is known as the rate of production of residual kinetic energy,

$$\mathcal{P}_r(\mathbf{x}, t) \equiv -\tau_{ij}^r \overline{S}_{ij}. \quad (7)$$

Here  $\overline{S}_{ij} \equiv (1/2)(\partial \overline{U}_i / \partial x_j + \partial \overline{U}_j / \partial x_i)$  is the rate of strain tensor due to the filtered field. When  $\mathcal{P}_r > 0$ , energy is lost from the filtered motions (in our case, large-scale flow above  $\ell_O$ ) and transferred to the residual motions (i.e., small-scale flow below  $\ell_O$ ). In other words, kinetic energy follows the usual notion of cascade, moving from large scales to small when  $\mathcal{P}_r > 0$ . Unlike the dissipation rate which is nonnegative, it is possible that  $\mathcal{P}_r < 0$  locally in the flow, i.e., there exists local back-scatter of energy within the flow, where energy is transferred from small scales to large, strengthening the large-scale mean flow at the expense of small-scale turbulence—we will discuss the implication of this phenomenon in the context of local SOC-like dynamics in Sec. III C. Note that the chosen filter scale,  $\ell_O$ , is observed to be two to three orders of magnitude smaller than the energy-containing, horizontal integral scale,  $\ell_h$  [24]. Therefore, small variations to the filter length (say, within the same order of magnitude of  $\ell_O$ ) are not expected to drastically alter the partition of energy between the filtered and residual fields, and thus small changes to the filter length would have a minimal effect on quantities such as  $\overline{S}_{ij}$  and Ri.

Another useful concept for the discussion in Sec. III D is one related to the eddy viscosity. Following Sec. 13.4 of Ref. [47], one can express  $\tau_{ij}^r$  using an eddy-viscosity model:

$$\tau_{ij}^r = -2\nu_e \overline{S}_{ij}, \quad (8)$$

where  $\nu_e(\mathbf{x}, t)$  is the eddy viscosity due to the residual motions. This definition of  $\nu_e$  assumes that the eddy viscosity is locally isotropic and is consistent with the notion that  $\ell_O$  is the approximate upper bound for the isotropic scales. Substituting Eq. (8) into Eq. (7) leads to

$$\mathcal{P}_r(\mathbf{x}, t) \equiv -\tau_{ij}^r \overline{S}_{ij} = 2\nu_e \overline{S}_{ij} \overline{S}_{ij}, \quad (9)$$

which allows one to evaluate  $\nu_e$  based on  $\mathcal{P}_r$  and  $\overline{S}_{ij}$ . It follows from Eq. (9) that  $\mathcal{P}_r$  and  $\nu_e$  have the same sign because  $\overline{S}_{ij} \overline{S}_{ij}$  is nonnegative. When  $\nu_e > 0$ , the residual motions diffuse the large-scale velocity gradients in the usual sense of diffusion; when  $\nu_e < 0$ , the large-scale velocity gradients are strengthened by the residual motions, while kinetic energy undergoes back-scatter from small to large scales. With the decomposition in Eq. (4) applied to the numerical data, one would have access to both  $\mathcal{P}_r$  and  $\nu_e$  as they vary in space and time. Statistics of these quantities will be examined in conjunction with Ri in the following section.

### III. RESULTS AND DISCUSSION

#### A. Statistical distribution of Ri

According to criterion 1 for SOC postulated by Ref. [4], the critical state, which is characterized by  $\text{Ri} \sim 1/4$ , acts as an attractor around which the turbulence self-organizes. While the overall

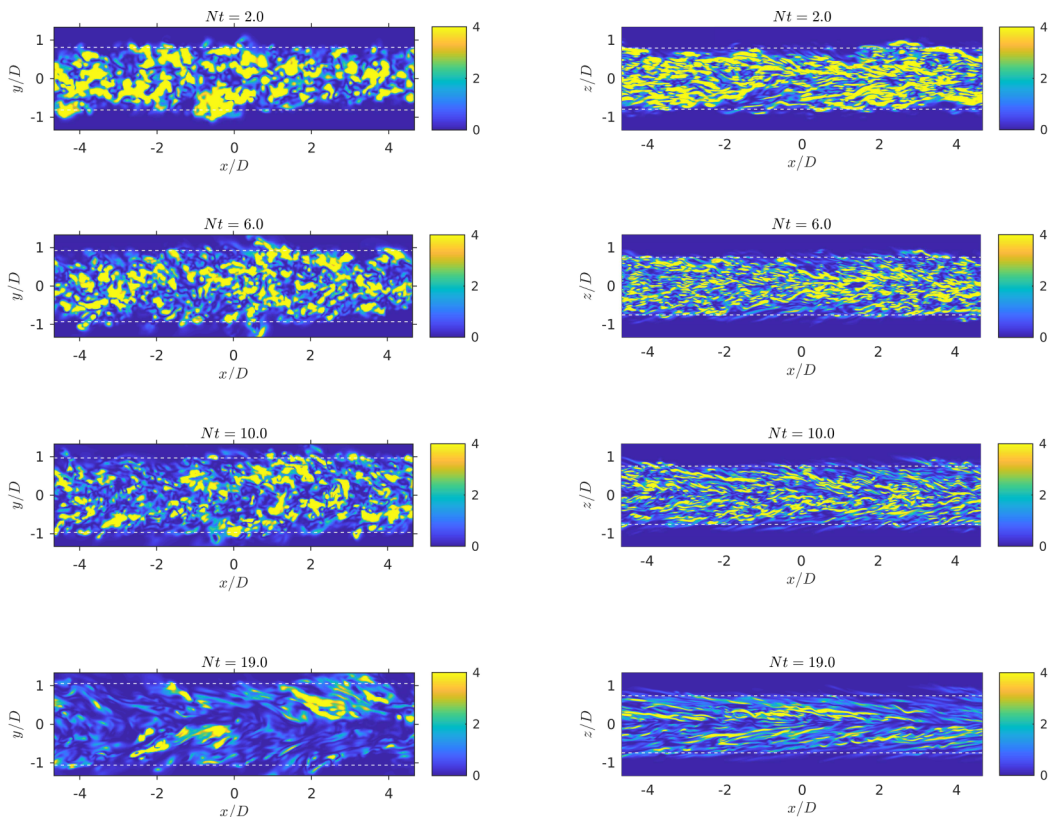


FIG. 4. Horizontal transects of  $1/Ri$  at the center  $oxy$  plane ( $z = 0$ ) shown for various times in the left column; vertical transects of  $1/Ri$  at the center  $oxz$  plane ( $y = 0$ ) shown in the right column. Thin dashed lines indicate the location where  $y = \pm 2L_H$  or  $z = \pm 2L_V$ . The color corresponding to  $Ri < 1/4$  is deliberately oversaturated to highlight regions of low stability. Images shown are close-up views of the central one half of the domain in the  $x$  direction,  $-(14/3)D < x < (14/3)D$ , and of a width and depth of  $(4/3)D$  on each side the wake centerline at  $(y, z) = (0, 0)$ .

distribution of  $Ri$  could vary subtly with the characteristics of forcing, the strongest turbulence robustly occurs around  $Ri \sim 1/4$ . For example, as shown in Fig. 2 of Ref. [4], while the PDF of  $Ri$  could vary slightly from year to year in the forced, equatorial current, the regions of strongest turbulence (as characterized by large turbulent heat flux) consistently produce a peak in the PDF at  $Ri \sim 1/4$ . In the quasiequilibrium situation examined by Ref. [3], the horizontally averaged  $Ri$  shows a peak in its occurrence around  $1/4$  for a long period of time, presumably due to the persistent actions of the Holmboe wave.

How does  $Ri$  behave in a strongly stratified decaying turbulence where neither external forcing nor a primary Holmboe wave instability is present? Here we examine the filtered field and calculate the large-scale gradient Richardson number,  $Ri$ , following Eq. (5). Sample horizontal and vertical transects of the  $1/Ri$  field are shown in Fig. 4. (The reason why  $1/Ri$  is considered in this paper is that we want to avoid singularities in  $Ri$  created when the squared vertical shear,  $S^2$ , i.e., the denominator when calculating  $Ri$ , becomes zero in the virtually quiescent region outside the wake's core region, causing inconvenience for analysis and visualization.) The color scheme in Fig. 4 is one such that regions corresponding to  $Ri < 1/4$  are highlighted in bright yellow. As the wake turbulence decays in time, the supercritical regions shown in yellow become increasingly sparse in space. As can be seen from the vertical transects, these yellow regions appear as thin layers

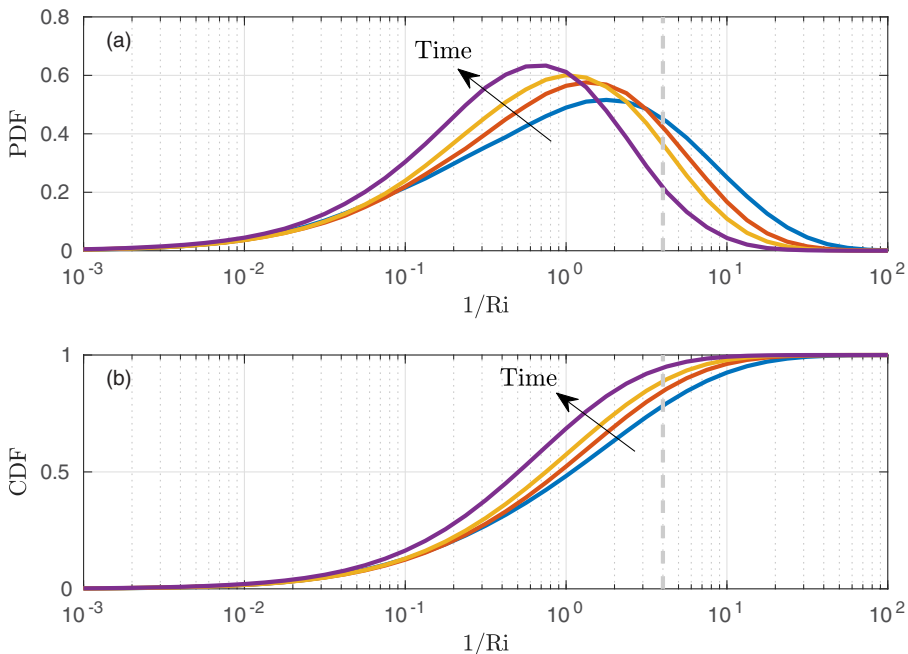


FIG. 5. Statistics of Ri: (a) PDF of  $1/Ri$  sampled in the wake core for all four cases and (b) CDF of  $1/Ri$ . The median values of Ri at each time are 0.923, 1.10, 1.34, and 1.98, respectively. Gray dashed lines in panels (a) and (b) indicate where  $Ri = 1/4$ ; the volume fraction in the wake core occupied by regions of  $Ri < 1/4$  at each time is 0.217, 0.155, 0.113, and 0.0550, respectively.

with finite length (in  $x$ ) and depth (in  $z$ ). The length is typically larger than the depth, which indicates a strong degree of anisotropy. As time goes by, the structures of thin vertical layers become increasingly organized—for the snapshot at  $Nt = 19$  (case D) specifically, regions of low Ri appear over the  $oxz$  plane in the form of wavelike undulations that are aligned in a preferred orientation on either side of the wake’s centerline. As shown in Fig. 4, the distribution of Ri is highly variable in space, which, to a certain extent, justifies the need for a locally defined Ri in the first place (Sec. II C).

Statistics of Ri are shown in Fig. 5(a) in terms of the PDF of the logarithm of  $1/Ri$  sampled within the wake’s core region defined by Eq. (2). The sampling bins are chosen uniformly at regular intervals of  $\log_{10} 1/Ri$ , and the PDF is calculated such that it satisfies the normalization condition  $\int_{-\infty}^{\infty} f(\chi) d\chi = 1$ , where  $\chi = \log_{10} 1/Ri$  and  $f(\chi)$  is the corresponding PDF. As the wake turbulence decays, the PDF shifts gradually to the left, meaning that Ri overall increases with time. Unlike Ref. [3] in which the horizontally averaged Ri centers around  $1/4$ , the peak of the local Ri shown in Fig. 5(a) consistently stays above  $1/4$ , which seemingly contradicts criterion 1 for SOC where Ri is required to be maintained around the critical value—this is an important issue and will be addressed in the following subsection. Figure 5(b), showing the cumulative distribution function (CDF) for  $1/Ri$ , suggests that a nontrivial portion of the flow volume remains occupied by regions of  $Ri < 1/4$ , even at the later times under consideration. While  $Re_b$  has decayed by about one order of magnitude from case A to case D (Fig. 2), the corresponding median Ri has increased only from 0.923 to 1.98 (Fig. 5), by approximately a factor of two.

### B. Dissipation vs Ri

When examining criterion 1 for SOC according to Ref. [4], it is important to note that the peak in the distribution of Ri is expected to be near  $1/4$ , not for the entire volume of the flow, but for regions

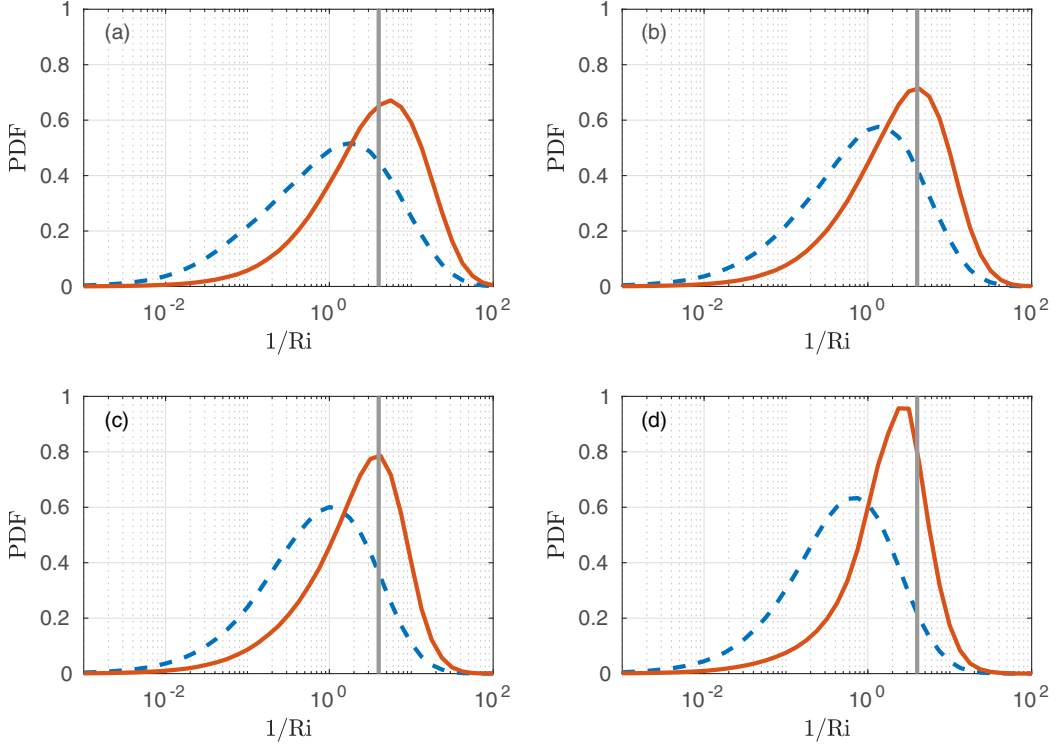


FIG. 6. PDF of  $1/Ri$  sampled for the entire wake core for all four cases, plotted with a blue dashed line, and the corresponding PDF subsampled for regions of the upper quartile of dissipation,  $\varepsilon(\mathbf{x}, t)$ , plotted in a red solid line. Grey vertical lines indicate where  $Ri = 1/4$ .

of the strongest turbulence. Indeed, for the oceanic measurements presented in Ref. [4], when  $Ri$  is subsampled for regions of upper quartile of the turbulent heat flux, the peak appears near  $Ri = 1/4$  (see their Fig. 2). A similar subsampling approach is applied to the wake data, which are shown in Fig. 6. While the PDF does not show a peak near  $1/4$  for the overall volume [Fig. 5(a)], it does move considerably closer to  $1/4$  for the most dissipative regions in the flow (characterized by upper quartile of  $\varepsilon$ ), which is consistent with the field data presented in Ref. [4]. This suggests that the wake turbulence, at least for the time period under consideration, does attract the most dissipative local turbulence events to occur around  $Ri = 1/4$ . Such a threshold behavior for  $Ri$  is an indication of self-organization of turbulence around some critical state in the strongly stratified wake.

The reason for the shift in the PDF in  $Ri$  (Fig. 6) upon subsampling is that region of low  $Ri$  (hence low stability) is naturally associated with high  $\varepsilon$  (i.e., vigorous turbulence). In Fig. 7 samples taken from the dissipation field (after taking the logarithm of the dissipation, to account for the vast range of  $\varepsilon$  and its highly nonuniform distribution in space) are shown in the same format as the plots for  $1/Ri$  shown in Fig. 4. Close inspection between the  $\varepsilon$  field (Fig. 7) and the  $1/Ri$  field (Fig. 4) reveals that regions of high  $1/Ri$  typically correlate with regions of high  $\varepsilon$ , which is as expected. The peak of the subsampled  $Ri$  PDF (Fig. 6) does deviate slightly from  $1/4$  for cases A and D; i.e., the peak  $Ri$  is slightly lower than  $1/4$  for case A, and slightly higher than  $1/4$  for case D. This could be an indication that the flow is transitioning in (case A) and out of (case D) a regime for which the self-organization is most relevant.

Figure 7 shows that, as the turbulence decays in the wake, the magnitude of  $\varepsilon$  decreases significantly (the same color scheme is used for all panels in Fig. 7 for ease of comparison). The differences between the structures shown by the horizontal and vertical transects become more

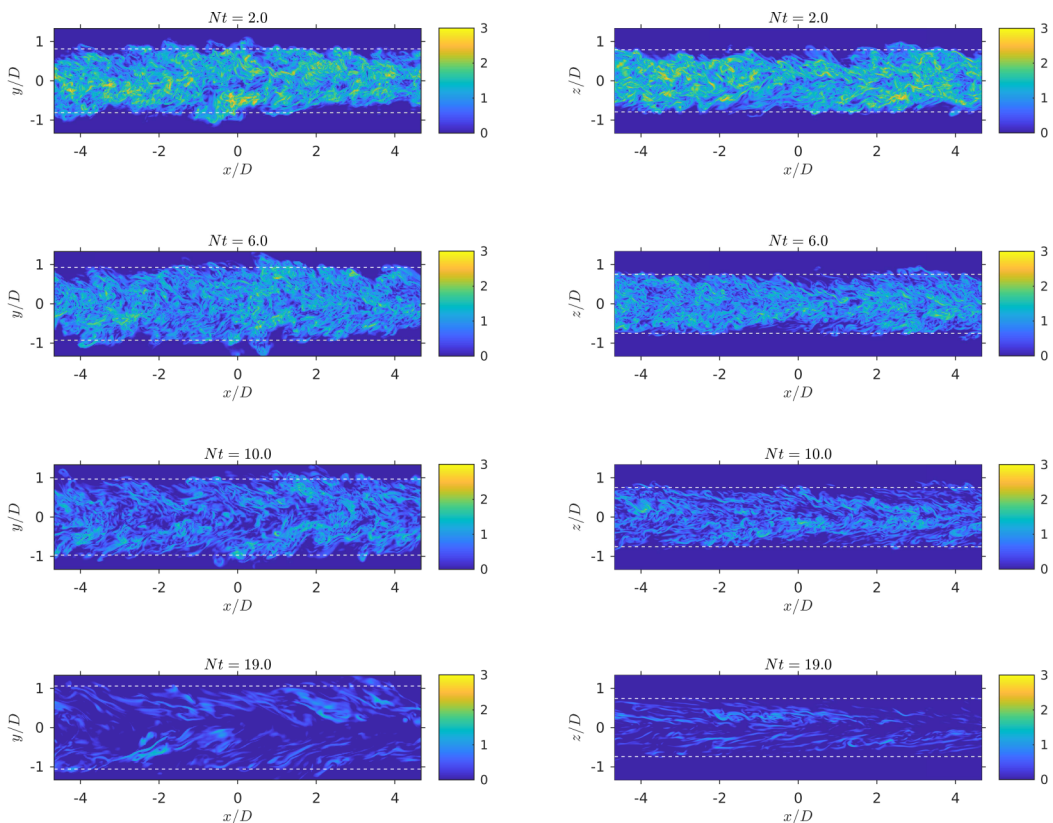


FIG. 7. Same layout as Fig. 4 but showing the  $oxy$  (left column) and  $oxz$  (right column) transects of  $\log_{10} \varepsilon/\nu N^2$  at each time.

pronounced for later cases, which results from the growing anisotropy in the flow, e.g., as evidenced by the decreasing values of  $Fr_h$  (Fig. 2). Relative to the fast decay in  $\varepsilon$ , the decay of  $1/Ri$  is slower, as evidenced by the prevalence of regions of  $Ri < 1/4$  shown in Fig. 4 and the slow shift of the solid orange curves shown in Fig. 6. This is critically due to the fact that the flow self-organizes into layered anisotropic structures to preserve the vertical shear, which is a fundamental characteristic of the strongly stratified turbulence regime [40,41,48] and could potentially be the manifestation of the underlying flow self-organization which attracts  $Ri$  to be around  $1/4$  (Fig. 6). The slow decay of  $1/Ri$  could, in turn, explain the observed reduced rate of turbulence decay in wakes (e.g., [21,49]) during the NEQ regime, as compared to the predictions based on axisymmetric self-similar profiles.

There exists a large volume of literature concerning  $\varepsilon$  and its relation to  $Ri$  (or expressed in terms of the squared vertical shear,  $\mathcal{S}^2$ , when  $N^2$  is a constant) in decaying stratified turbulence (e.g., Refs. [50–54]), where both quantities ( $\varepsilon$  and  $Ri$ ) are examined in the volume-averaged sense. Here we adopt an alternative approach in which  $\varepsilon$  is conditionally sampled over regions of various value of  $1/Ri$  from the same flow snapshot, yielding the conditional mean of  $\varepsilon$  as a function of  $1/Ri$ ,  $\tilde{\varepsilon}(1/Ri)$ , which is shown in Fig. 8. The conditional mean,  $\tilde{\varepsilon}$ , is observed to increase monotonically with  $1/Ri$ , consistent with the correlation between high  $\varepsilon$  and low  $Ri$  observed in Figs. 4 and 7. Each case under examination yields an individual curve shown in the two panels of Fig. 8, where different normalizations for  $\tilde{\varepsilon}$  are used. When  $\tilde{\varepsilon}$  is normalized by  $\nu N^2$ , as in Fig. 8(a), the variable plotted in the vertical axis can be effectively considered as the conditionally sampled buoyancy Reynolds number,  $Re_b$ , according to local value of  $1/Ri$ .

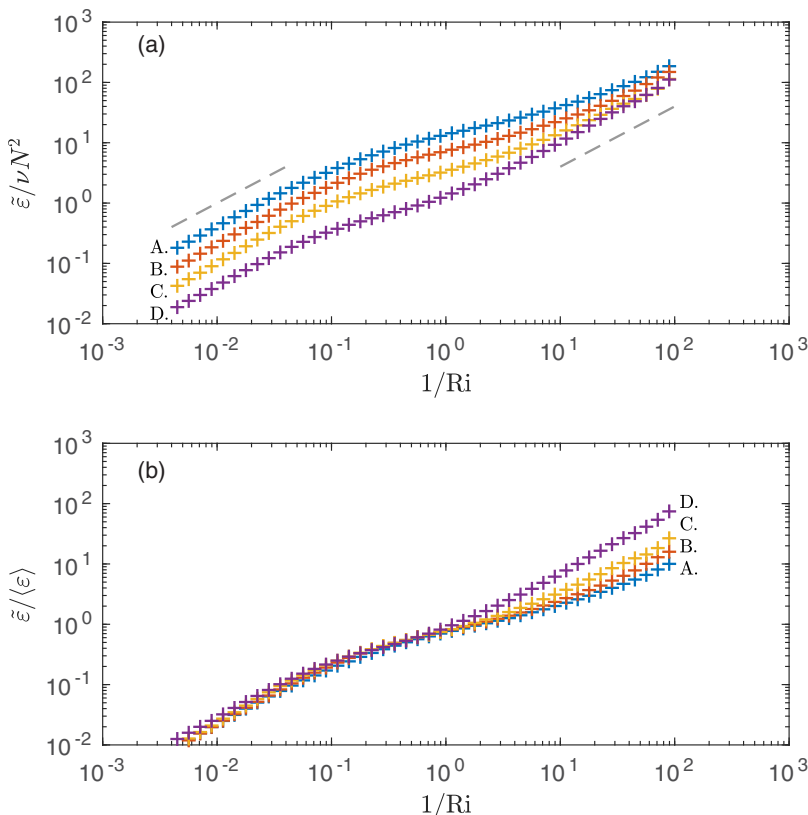


FIG. 8. Conditional mean of (a)  $\bar{\varepsilon}/\nu N^2$  and (b)  $\bar{\varepsilon}/\langle\varepsilon\rangle$  as a function of  $1/\text{Ri}$  shown for all four cases under consideration. Dashed lines in panel (a) indicate linear scalings between the two variables,  $\bar{\varepsilon}/\nu N^2 \propto 1/\text{Ri}$ .

Two limits seem to emerge in Fig. 8(a): In the most stable limit,  $1/\text{Ri} \ll 1$ , the relation between  $\bar{\varepsilon}/\nu N^2$  and  $1/\text{Ri}$  is close to a linear one. This is reminiscent of the approximation often made in a strongly anisotropic situation to attribute dissipation entirely to vertical shear,  $\varepsilon \sim \nu S^2$  (e.g., Ref. [52]), which then leads to  $\text{Re}_b \sim \text{Ri}^{-1}$ , a relation that is observed to hold for strong stratification and weak turbulence,  $\text{Re}_b \sim O(1)$  or smaller [53,54]. The vertical offset for different cases in this limit, as seen in Fig. 8(a), seems to scale with the bulk dissipation rate; i.e., when  $\bar{\varepsilon}$  is instead normalized by the volume-averaged dissipation,  $\langle\varepsilon\rangle$ , as in Fig. 8(b), the curves all collapse for small values of  $1/\text{Ri}$  up to  $1/\text{Ri} \sim O(1)$ . In the most unstable limit,  $1/\text{Ri} \gg 1$ , the curves seem to approach some degree of convergence, as seen in Fig. 8(a). In this limit, at least for cases corresponding to later times, the relation between  $\bar{\varepsilon}/\nu N^2$  and  $1/\text{Ri}$  seems to approach the linear scaling again. This could potentially be linked to the weakly stratified limit of Monin-Obukhov scaling for constant-flux layers (see, e.g., Sec. 6.3 of Ref. [9]), for which  $\text{Re}_b \sim \text{Ri}^{-1}$  also holds, albeit for a different reason from the stable limit. In summary, the results shown in Fig. 8 indicate that the magnitude of the dissipation  $\varepsilon$  could be dictated by different dynamics towards the two limits,  $\text{Ri} \gg 1$  and  $\text{Ri} \ll 1$ , respectively, as  $\text{Ri}$  deviates from the critical value of  $1/4$ . The local  $\text{Ri}$ , which is to be interpreted as a measure of stability, does give a reasonably good indication for how vigorous the turbulence is, as characterized by the local  $\varepsilon$ . However, the quantitative relation between  $\text{Ri}$  and  $\bar{\varepsilon}/\nu N^2$  is most certainly not unique, as it could depend on the definition of these quantities; in fact, a large degree of scattering can be observed from oceanic measurements (see Fig. 17 of [55] and Fig. 15 of [56])—the authors of Ref. [56] rightfully cautioned that “with no further understanding of the forcing, it is impossible to generalize our results.”

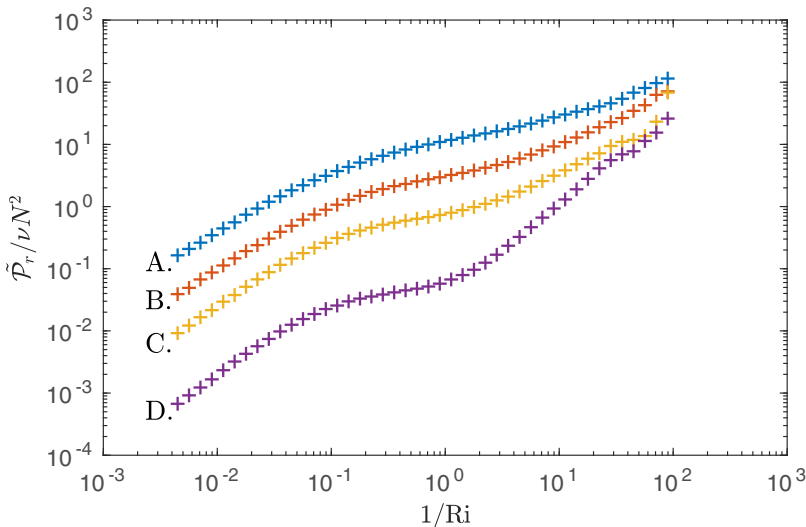


FIG. 9. Conditional mean of the production of residual kinetic energy,  $\tilde{\mathcal{P}}_r(1/\text{Ri})$ , when normalized by  $\nu N^2$ , as it varies with  $1/\text{Ri}$ .

### C. Production of residual kinetic energy vs Ri

Now we have seen evidence for flow self-organization in the wake in terms of the threshold behavior of  $\text{Ri}$  (Fig. 6), but how are the SOC-like dynamics maintained in a decaying flow without external forcing? Reference [4] postulated a dynamical cycle which depends critically on an external forcing which restores vertical mean shear when  $\text{Ri}$  rises above  $1/4$ , as well as turbulent diffusion which smooths out the mean shear and causes  $\text{Ri}$  to increase when turbulence kinetic energy (TKE) is at a high level (see their Fig. 3). The overall TKE undergoes a phase of growth when  $\text{Ri} < 1/4$  and a phase of decay when  $\text{Ri} > 1/4$ , while the critical state at  $\text{Ri} = 1/4$  characterizes the transition between the phases. In the present analysis, however, regions of various  $\text{Ri}$  coexist within the volume of flow (Fig. 4) at the same time. Our focus, again, is on how the local  $\text{Ri}$ , which characterizes the local stability property of the large-scale flow (specifically, scales above the Ozmidov scale,  $\ell_O$ ; see Sec. II C) affects the local energetics.

Here we examine how  $\text{Ri}$  affects the production of the residual kinetic energy,  $\mathcal{P}_r$ , which is the local rate of energy transfer from the large to small scales. When  $\mathcal{P}_r > 0$ , the local dynamics, i.e., kinetic energy being transferred downscale through a forward cascade to smaller scales, are analogous to the situation in Ref. [4] where the instability triggers turbulence and allows TKE to grow when  $\text{Ri} < 1/4$ ; when  $\mathcal{P}_r < 0$ , back-scatter (or inverse cascade) of kinetic energy exists locally and energizes the large-scale flow, which is analogous to the effect of external forcing in Ref. [4], i.e., the surface wind restores the mean vertical shear and reduces  $\text{Ri}$ , accompanied by decaying TKE when  $\text{Ri} > 1/4$ . In Ref. [4] the  $\text{Ri}$  value at a given time is a sufficient indicator for whether turbulence grows or decays— analogously, could the local  $\text{Ri}$  be such a indicator for whether  $\mathcal{P}_r$  is positive or negative locally in the wake flow?

To answer this question, we examine Fig. 9, which shows the conditional mean of  $\mathcal{P}_r$ , denoted as  $\tilde{\mathcal{P}}_r$ , as it varies with  $1/\text{Ri}$ . First and foremost,  $\tilde{\mathcal{P}}_r$  is observed to be positive for all cases under consideration and for all  $\text{Ri}$  sampled, suggesting that on average, the wake flow transfers energy from large to small scales, producing a forward cascade overall regardless of the magnitude of  $\text{Ri}$ . The direction of energy transfer, which is described by the sign of  $\tilde{\mathcal{P}}_r$ , is not determined by  $\text{Ri}$ , unlike the case in Ref. [4] where the instantaneous  $\text{Ri}$  alone is a sufficient indicator for the grow or decay of overall TKE at a given time. Similar to the trend shown in Fig. 8 for dissipation,  $\tilde{\mathcal{P}}_r$  increases monotonically with  $1/\text{Ri}$ . Statistically, regions of low  $\text{Ri}$  are associated with a large

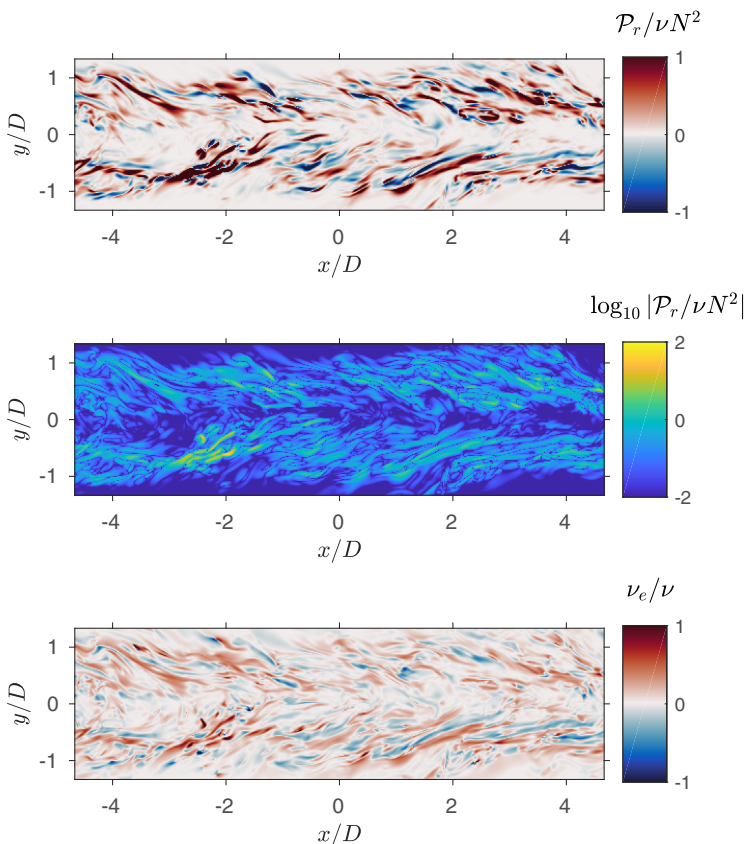


FIG. 10. Horizontal transects at the center  $oxy$  plane ( $z = 0$ ) shown for case D ( $Nt = 19.0$ ) for  $\mathcal{P}_r/\nu N^2$  (top),  $\log_{10} |\mathcal{P}_r/\nu N^2|$  (middle) and  $\nu_e/\nu$  (bottom), respectively. Images shown are close-up views of the central one half of the domain in the  $x$  direction, and of a width of  $(4/3)D$  on each side of the wake centerline.

net rate of energy transfer to the small scales, and vice versa. The energy transferred to scales below  $\ell_O$  is expected to be transferred further downscale via the inertial subrange that could exist (when  $Re_b > 20$ ; see, e.g., Ref. [57]) between  $\ell_O$  and the Kolmogorov scale,  $\ell_K$ , and eventually gets dissipated by viscosity.

The distribution of  $\mathcal{P}_r$  in physical space is examined in Fig. 10. The top panel shows a sample horizontal transect of  $\mathcal{P}_r$  taken for case D ( $Nt = 19.0$ ), where both positive and negative  $\mathcal{P}_r$  can be observed. Regions of large magnitude of  $\mathcal{P}_r$ , both positive and negative, tend to occur in wavelike alternate stripes which are indicated by a dark red or blue color. The peak magnitude of positive and negative  $\mathcal{P}_r$  are in fact comparable, as can be seen in the middle panel of Fig. 10, where the logarithm of the magnitude of  $\mathcal{P}_r$  is shown. This suggests that forward and inverse cascades could be equally energetic at different locations within the flow—the energy transfer is a two-way exchange driven by local processes, which is analogous to the observation of both positive and negative shear production in breaking internal waves (see Fig. 11 of Ref. [58]). Overall, the upscale and downscale transfer reaches a delicate balance and produces a net positive  $\mathcal{P}_r$  (forward cascade) as shown in Fig. 9.

#### D. Eddy viscosity vs Ri

In the previous subsection, we have seen that the conditional mean  $\tilde{\mathcal{P}}_r$  is positive regardless of the value of Ri. Now what exactly is the role of the critical  $Ri = 1/4$  in the maintenance of local SOC dynamics? We continue to investigate this issue using the eddy viscosity,  $\nu_e$ , which can be calculated

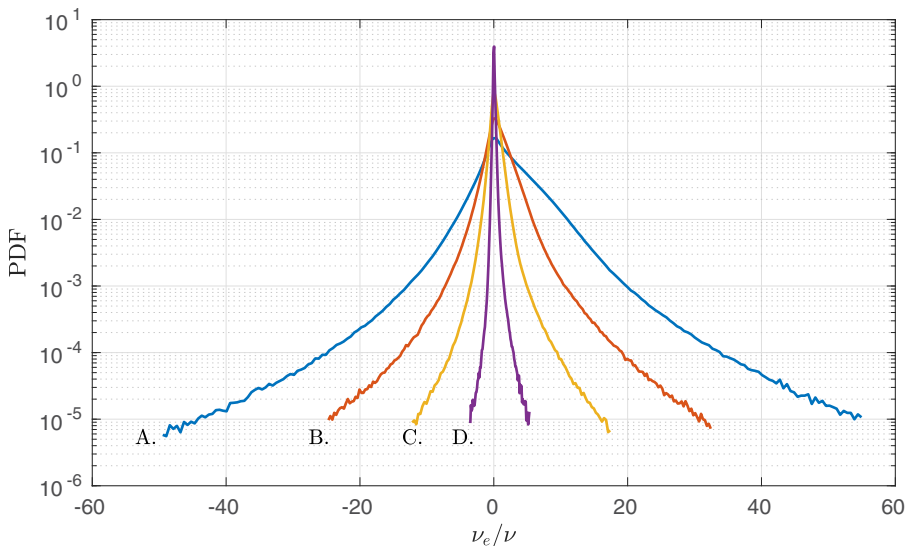


FIG. 11. PDF of the normalized eddy viscosity,  $v_e/\nu$ , for the four cases under consideration.

from  $\mathcal{P}_r$  and the filtered rate of strain tensor,  $\bar{S}_{ij}$ , via Eq. (9). By construction [see Eq. (9)],  $v_e$  and  $\mathcal{P}_r$  have the same sign and convey consistent physical interpretations.

Figure 11 shows the PDF of  $v_e$  (normalized by the molecular viscosity,  $\nu$ ) sampled within the wake's core region. For all four cases considered, the PDF peaks at  $v_e/\nu = 0$ , with the height of the spike increasing with time, which is as a result of the growing degree of intermittency in the flow—a larger fraction of the flow volume becomes effectively laminar-like ( $v_e \rightarrow 0$ ) as the turbulence decays (Fig. 7). The PDF decreases from its peak at  $v_e/\nu = 0$  towards both positive and negative values of  $v_e$ . The range of  $v_e/\nu$  corresponding to a given PDF level shrinks with time, e.g., the range of  $v_e/\nu$  corresponding to a PDF greater or equal to  $10^{-5}$  is approximately  $[-44, 55]$  for case A, and  $[-3.5, 5.4]$  for case D. While the curves look largely symmetric about  $v_e/\nu = 0$ , the distributions all have a noticeable bias towards the positive  $v_e/\nu$ . The mean of  $v_e$  stays positive in all cases, which is consistent with the overall positive  $\mathcal{P}_r$  observed in Fig. 9. Statistically, the overall effect of  $v_e$  is diffusive ( $v_e > 0$ ), i.e., to smooth out the large-scale velocity gradients; locally, the effect of  $v_e$  can be either diffusive or counterdiffusive, the latter meaning that large-scale shear is enhanced by the negative eddy diffusivity or, equivalently, by the back-scatter associated with the negative  $\mathcal{P}_r$  to inject energy into the large-scale motions (Sec. II C). The presence of locally negative eddy viscosity that restores shear, or back-scatter of kinetic energy to large scales, could be a key feature that enables the local dynamics to spontaneously bring the local shear back beyond the critical state at  $\text{Ri} = 1/4$ , in order to trigger turbulence and complete the local dynamical cycle.

For the above hypothesis to be valid, one would expect large magnitude of  $v_e/\nu$ , both positive and negative at various phases of the local cycle, to occur frequently around the critical state at  $\text{Ri} = 1/4$ . This is indeed the case, as shown by the joint PDF between  $v_e/\nu$  and the logarithm of  $1/\text{Ri}$  shown in Fig. 12. For all cases, the peak of the joint PDF occurs along the horizontal axis ( $v_e = 0$ ) and at comparable values of  $\text{Ri}$  across all cases (since the PDF of  $\text{Ri}$  itself changes minimally over time; see Fig. 5). Along the vertical axis, the range of  $v_e/\nu$  observed in each case is reduced considerably over time, consistent with Fig. 11, which results from the decay of turbulence. For a given value of  $\text{Ri}$ , as the magnitude of  $v_e/\nu$  increases, the PDF decreases significantly, as represented by contour lines of reduced PDF levels located farther away from the peak. While the shape of the area enclosed by each contour line is largely symmetric, the center of mass is slightly biased towards  $v_e > 0$ . As the turbulence decays, the occurrence of large magnitude of  $v_e/\nu$  becomes less frequent; the asymmetry in the contour line shape, especially for the contour levels away from

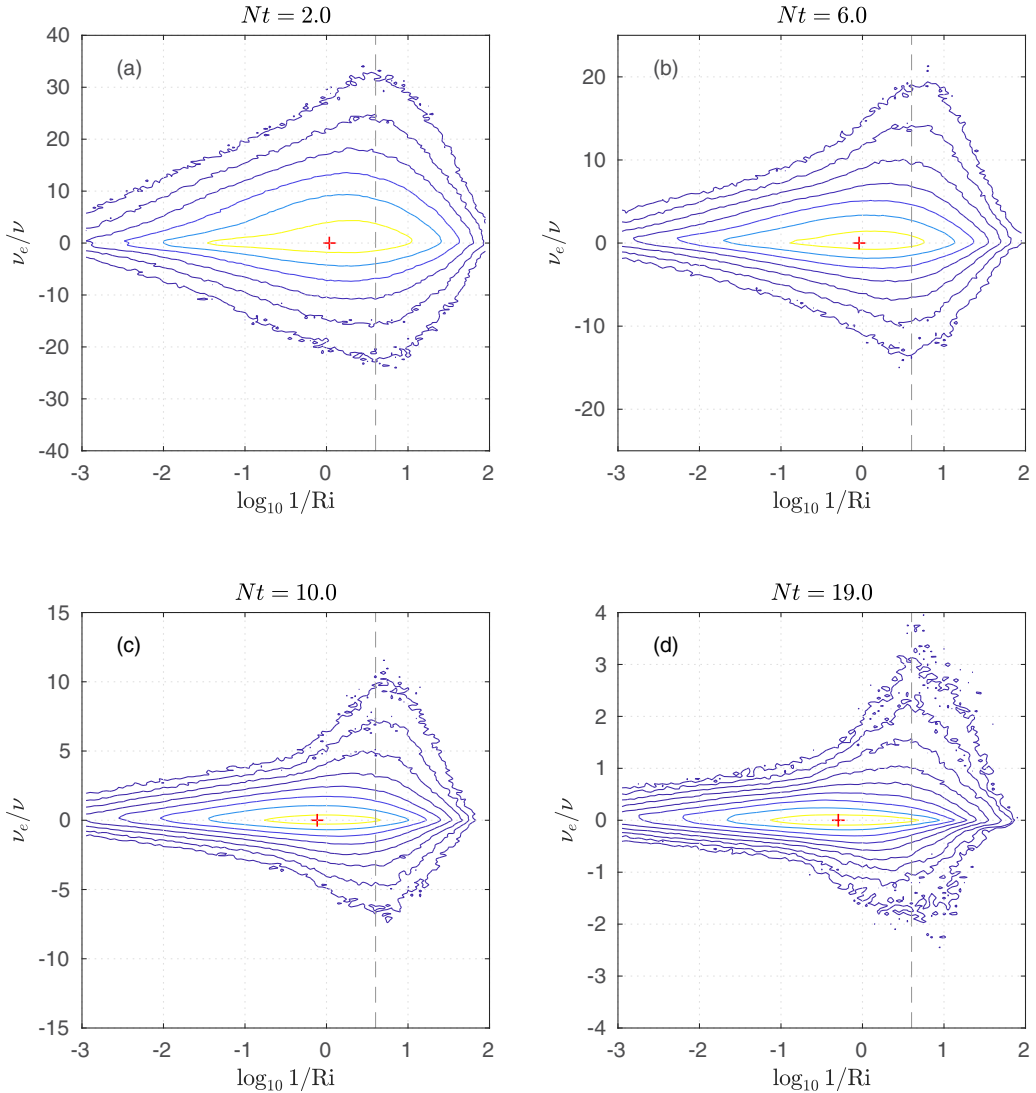


FIG. 12. Joint PDF between the normalized eddy viscosity,  $v_e/\nu$ , and the logarithm of  $1/Ri$ , plotted as contour lines for each of the four cases under consideration. The highest contour level (in yellow) corresponds to a value of  $\{\sqrt{10}, 10, 10\sqrt{10}, 100\} \times 10^{-2}$  for cases A, B, C, and D, respectively; for each contour level away from the center, the corresponding PDF is reduced by a factor of  $1/\sqrt{10}$ . The red cross plotted on the horizontal axis corresponds to the median value of  $Ri$ . The gray vertical dashed line corresponds to  $Ri = 1/4$ .

the peak, also grows in time—a protrusion of the outermost contour lines into the larger magnitude of  $v_e/\nu$ , both positive and negative, can clearly be observed in cases B, C, and D. The  $Ri$  value that corresponds to the tip of the protrusion, allowing the PDF to access the largest magnitude of  $v_e/\nu$ , appears markedly close to the critical value,  $Ri = 1/4$ . Around this critical state, one observes the peak occurrence of large magnitudes of  $v_e$ , both diffusive and counterdiffusive. There appears to be an intensified action of turbulence, which could either diminish or strengthen the large-scale shear locally, that occurs around  $Ri = 1/4$ , as evidenced by all cases shown in Fig. 12. This constitutes an essential characteristic of the decaying strongly stratified turbulence that potentially allows the self-organization of flow around  $Ri \sim 1/4$  to be maintained locally and spontaneously in the flow.

#### IV. CONCLUDING REMARKS

In this paper we report threshold behavior of the local gradient Richardson number,  $Ri$ , in strongly stratified turbulence identified from numerical data (Sec. II A) of a turbulent wake in a uniformly stratified fluid. The wake flow is strongly stratified, as characterized by  $Fr_h \sim O(0.01)$ , and sufficiently energetic such that  $Re_b > 1$  (Sec. II B) for the four cases under consideration. Turbulence within this strongly stratified regime [40,41] spontaneously forms layered anisotropic structures [42,43] within which local dynamics develop and self-maintain. We apply a flow decomposition (Sec. II C) that separates the large scales above the Ozmidov scale ( $\ell_o$ ) that are directly impacted by stratification, and the small scales below  $\ell_o$  that are dominated by inertia and viscous processes. As the turbulence decays, the median value of  $Ri$  remains approximately the same to within a factor of two (Fig. 5), while  $Re_b$  decays by approximately one order of magnitude. The distribution of local  $Ri$  associated with the upper quartile dissipation peaks around  $1/4$  (Fig. 6). Regions of small  $Ri$  are typically associated with large dissipation (Fig. 8) and large net transfer of energy from large to small scales (Fig. 9). Regions of  $Ri$  values around  $1/4$  are also where the eddy viscosity (both positive and negative) is observed to be of the largest magnitude (Fig. 12). The observed threshold behavior of  $Ri$  reveals the self-organization of flow around a certain critical state in strongly stratified wake turbulence.

The results presented in this paper complement two prior papers [3,4] applying the concept of SOC to stably stratified turbulence. We observe self-organization of flow in decaying strongly stratified turbulence in the absence of a sharp density interface that supports a certain type of primary instability as in Ref. [3], or an external forcing that acts to periodically reduce  $Ri$  as in Ref. [4]. This indicates that self-organization of flows around a certain critical state can be a generic property of stratified turbulence in certain regimes, not necessarily relying on a specific external driving mechanism. The distribution of eddy viscosity reported in Sec. III D reveals a possible internal mechanism through which the flow self-organizes around the critical state. However, one ought not to expect such dynamics to be relevant in all situations—in the specific context of the stratified wake, we seem to observe an overlap between the flow’s self-organization and the strongly stratified or the LAST regime [40–42], which is accessible only for a certain range of wake parameters [24]. It does not seem unreasonable to expect the self-organization to be irrelevant for wakes which are either too weakly stratified (e.g., boundary-forced flows as reviewed in Sec. 5.1 of Ref. [59]), where  $Ri$  never exceeds  $1/4$ , or dominated by viscous effects and has no sufficient dynamical range for overturns, such as those in the quasi-two-dimensional regime in late wakes [21,22]. While the strongly stratified wake turbulence is grossly out of equilibrium overall, we do observe some signatures of quasiequilibrium on a local and perhaps transient level, e.g., the intense two-way exchange of energy between large and small scales shown in Fig. 10, and the broad distribution of eddy viscosity over both positive and negative values as shown in Fig. 11. This suggests that the applicability of the SOC or MI paradigm might not be limited to globally balanced or quasibalanced flows [3,4]—it could potentially be useful for addressing numerous imbalanced scenarios in geophysical flows [19,43] as well.

In contrast to the clear-cut separation of growth and decay of TKE by  $Ri \sim 1/4$  proposed in Ref. [4], the role played by the local  $Ri$  in the wake is a subtle one, i.e., the local  $Ri$  itself does not necessarily dictate pointwise whether the large-scale shear is enhanced or reduced by the turbulence (Fig. 12), while statistically there does exist a positive correlation between the local value of  $1/Ri$  and the net forward cascade of kinetic energy (Fig. 9). We observe the self-sustaining dynamics to be maintained in a local sense, driven by an intense two-way exchange of energy between the large and small scales that occurs around the critical  $Ri = 1/4$ . Key to this characterization is the occurrence of large magnitude of eddy viscosity, both positive and negative, conspicuously close to this supposed critical state (Fig. 12). In a sense, the negative eddy viscosity, which can be thought to be intrinsically linked to the spontaneous layering of vertical shear in the strongly stratified or the LAST regime [40,41], is analogous to the counterdiffusive behavior of turbulent mixing, which can lead to the layering of density within certain regions of the  $(Ri, Re_b)$  parameter space [60,61]

through the mechanism proposed by Phillips and Postmentier [62,63]—for the latter mechanism to be functional, it has been shown that the Prandtl number may play a role (see, e.g., Refs. [35,61]). The coupling between the turbulent mixing of momentum and scalar in these self-organized flows could be a topic of future research. Furthermore, it remains a perplexing issue why  $Ri = 1/4$ , a criterion developed for a specific set of conditions [6,7] that do not apply here, stays relevant for a complex multiscale turbulent flow under consideration.

In closing, it is worth emphasizing that it is not the aim of this paper to prove that the dynamics exhibited by the strongly stratified turbulence examined *are* categorically the manifestation of SOC. Our main aim here has been to show that the threshold behavior of  $Ri$  does exist in a nonequilibrium flow, a characteristic that is indeed reminiscent of criterion 1 for SOC outlined by Ref. [4]. Flow characteristics reported in Secs. III C and III D shed light on how the flow self-organizes such that  $Ri$  tends to stay around  $1/4$ , which forms the main discovery from our analysis. Efforts have been made to examine criterion 2 for SOC [4] concerning the power-law distribution of event sizes; however, it turns out that the definition used by Ref. [3] to characterize the event size would lead to spuriously large length scales which are difficult to interpret physically. As formulating the event size is a nontrivial task in itself and outside the scope of this paper, we opt to defer such efforts to future studies. It is anticipated that a clear-cut test of the length scale distribution against criterion 2 for SOC would require a large separation between the relevant length scales, such as the energy-containing, Ozmidov and Kolmogorov lengths, which would require more computational resources than currently available to us. A top priority for future research is thus to characterize the various length scales in a simulation with large  $Re_b$  ( $Re_b > 20$ ) yet small  $Fr_h$  [ $Fr_h \sim O(0.01)$ ] in order to definitively prove the existence of SOC (or otherwise) in stratified turbulence.

#### ACKNOWLEDGMENTS

Support by the Natural Sciences and Engineering Research Council of Canada (NSERC) through a Discover Grant (RGPIN-2018-04329) and by the Marine Environmental Observation, Prediction and Response (MEOPAR) network through an early-career researcher grant is gratefully acknowledged. This research was enabled in part by resources provided by Compute Canada and by the Advanced Research Computing (ARC) cluster at the University of Calgary. I would like to thank an anonymous reviewer of a previous version of this manuscript whose thoughtful comments helped me improve this work significantly.

- 
- [1] P. Bak, C. Tang, and K. Wiesenfeld, Self-Organized Criticality: An Explanation of the  $1/f$  Noise, *Phys. Rev. Lett.* **59**, 381 (1987).
  - [2] G. Pruessner, *Self-organised Criticality: Theory, Models and Characterisation* (Cambridge University Press, Cambridge, 2012).
  - [3] H. Salehipour, W. R. Peltier, and C. P. Caulfield, Self-organized criticality of turbulence in strongly stratified mixing layers, *J. Fluid Mech.* **856**, 228 (2018).
  - [4] W. D. Smyth, J. D. Nash, and J. N. Moum, Self-organized criticality in geophysical turbulence, *Sci. Rep.* **9**, 1 (2019).
  - [5] G. P. Chini, G. Michel, K. Julien, C. B. Rocha, and C. P. Caulfield, Exploiting self-organized criticality in strongly stratified turbulence, *J. Fluid Mech.* **933**, A22 (2022).
  - [6] J. W. Miles, On the stability of heterogeneous shear flows, *J. Fluid Mech.* **10**, 496 (1961).
  - [7] L. N. Howard, Note on a paper of John W. Miles, *J. Fluid Mech.* **10**, 509 (1961).
  - [8] J. S. Turner, *Buoyancy Effects in Fluids* (Cambridge University Press, Cambridge, 1973).
  - [9] Q. Zhou, J. R. Taylor, and C. P. Caulfield, Self-similar mixing in stratified plane Couette flow for varying Prandtl number, *J. Fluid Mech.* **820**, 86 (2017).
  - [10] S. A. Thorpe and Z. Liu, Marginal instability? *J. Phys. Oceanogr.* **39**, 2373 (2009).
  - [11] W. D. Smyth and J. N. Moum, Marginal instability and deep cycle turbulence in the eastern equatorial Pacific Ocean, *Geophys. Res. Lett.* **40**, 6181 (2013).

- [12] W. D. Smyth and J. R. Carpenter, *Instability in Geophysical Flows* (Cambridge University Press, Cambridge, 2019).
- [13] W. D. Smyth, H. T. Pham, J. N. Moum, and S. Sarkar, Pulsating turbulence in a marginally unstable stratified shear flow, *J. Fluid Mech.* **822**, 327 (2017).
- [14] M. J. Aschwanden, A macroscopic description of a generalized self-organized criticality system: Astrophysical applications, *Astrophys. J.* **782**, 54 (2014).
- [15] D. Hebert, D. R. Caldwell, C. A. Paulson, and J. N. Moum, Turbulence and internal waves at the Equator. Part II: Details of a single event, *J. Phys. Oceanogr.* **22**, 1346 (1992).
- [16] J. N. Moum, J. D. Nash, and W. D. Smyth, Narrowband oscillations in the upper equatorial ocean. Part I: Interpretation as shear instabilities, *J. Phys. Oceanogr.* **41**, 397 (2011).
- [17] H. Van Haren, L. Gostiaux, E. Morozov, and R. Tarakanov, Extremely long Kelvin–Helmholtz billow trains in the Romanche fracture zone, *Geophys. Res. Lett.* **41**, 8445 (2014).
- [18] J. Tu, D. Fan, Q. Lian, Z. Liu, W. Liu, A. Kaminski, and W. D. Smyth, Acoustic observations of Kelvin–Helmholtz billows on an estuarine lutocline, *J. Geophys. Res. Oceans* **125**, e2019JC015383 (2020).
- [19] W. D. Smyth, Marginal instability and the efficiency of ocean mixing, *J. Phys. Oceanogr.* **50**, 2141 (2020).
- [20] A. Mashayek, L. E. Baker, B. B. Cael, and C. P. Caulfield, A marginal stability paradigm for shear-induced diapycnal turbulent mixing in the ocean, *Geophys. Res. Lett.* **49**, e2021GL095715 (2022).
- [21] G. R. Spedding, The evolution of initially turbulent bluff-body wakes at high internal Froude number, *J. Fluid Mech.* **337**, 283 (1997).
- [22] P. J. Diamessis, G. R. Spedding, and J. A. Domaradzki, Similarity scaling and vorticity structure in high-Reynolds-number stably stratified turbulent wakes, *J. Fluid Mech.* **671**, 52 (2011).
- [23] Q. Zhou, Far-field evolution of turbulence-emitted internal waves and Reynolds number effects on a localized stratified turbulent flow, Ph.D. thesis, Cornell University (2015).
- [24] Q. Zhou and P. J. Diamessis, Large-scale characteristics of stratified wake turbulence at varying Reynolds number, *Phys. Rev. Fluids* **4**, 084802 (2019).
- [25] B. Halawa, S. Merhi, C. Tang, and Q. Zhou, Three-dimensional visualization of stratified turbulent wakes at varying Reynolds number, *J. Vis.* **23**, 437 (2020).
- [26] P. J. Diamessis, J. A. Domaradzki, and J. S. Hesthaven, A spectral multidomain penalty method model for the simulation of high Reynolds number localized incompressible stratified turbulence, *J. Comput. Phys.* **202**, 298 (2005).
- [27] T. Watanabe, J. J. Riley, S. M. de Bruyn Kops, P. J. Diamessis, and Q. Zhou, Turbulent/non-turbulent interfaces in wakes in stably stratified fluids, *J. Fluid Mech.* **797**, R1 (2016).
- [28] Q. Zhou and P. J. Diamessis, Surface manifestation of internal waves emitted by submerged localized stratified turbulence, *J. Fluid Mech.* **798**, 505 (2016).
- [29] K. L. Rowe, P. J. Diamessis, and Q. Zhou, Internal gravity wave radiation from a stratified turbulent wake, *J. Fluid Mech.* **888**, A25 (2020).
- [30] W. D. Smyth and J. N. Moum, Length scales of turbulence in stably stratified mixing layers, *Phys. Fluids* **12**, 1327 (2000).
- [31] H. Salehipour, W. R. Peltier, and A. Mashayek, Turbulent diapycnal mixing in stratified shear flows: the influence of Prandtl number on mixing efficiency and transition at high Reynolds number, *J. Fluid Mech.* **773**, 178 (2015).
- [32] J. A. Redford, T. S. Lund, and G. N. Coleman, A numerical study of a weakly stratified turbulent wake, *J. Fluid Mech.* **776**, 568 (2015).
- [33] J. P. Boyd, *Chebyshev and Fourier Spectral Methods* (Dover Publications, Mineola, New York, 2001).
- [34] J. R. Taylor, Numerical simulations of the stratified oceanic bottom boundary layer, Ph.D. thesis, University of California, San Diego (2008).
- [35] Q. Zhou, J. R. Taylor, C. P. Caulfield, and P. F. Linden, Diapycnal mixing in layered stratified plane Couette flow quantified in a tracer-based coordinate, *J. Fluid Mech.* **823**, 198 (2017).
- [36] S. A. Orszag and Y.-H. Pao, Numerical computation of turbulent shear flows, *Adv. Geophys.* **18**, 225 (1975).

- [37] J. J. Riley and E. Lindborg, Recent progress in stratified turbulence, in *Ten Chapters in Turbulence*, edited by P. A. Davidson, Y. Kaneda, and K. R. Sreenivasan (Cambridge University Press, Cambridge, 2012), pp. 269–317.
- [38] M. L. Waite, Stratified turbulence at the buoyancy scale, *Phys. Fluids* **23**, 066602 (2011).
- [39] J. J. Riley, R. W. Metcalfe, and M. A. Weissman, Direct numerical simulations of homogeneous turbulence in density-stratified fluids, in *AIP Conf. Proc. on Nonlinear Properties of Internal Waves*, edited by J. B. West (American Institute of Physics, College Park, Maryland, 1981), pp. 79–112.
- [40] P. Billant and J.-M. Chomaz, Self-similarity of strongly stratified inviscid flows, *Phys. Fluids* **13**, 1645 (2001).
- [41] G. Brethouwer, P. Billant, E. Lindborg, and J.-M. Chomaz, Scaling analysis and simulation of strongly stratified turbulent flows, *J. Fluid Mech.* **585**, 343 (2007).
- [42] M. Falder, N. J. White, and C. P. Caulfield, Seismic imaging of rapid onset of stratified turbulence in the South Atlantic Ocean, *J. Phys. Oceanogr.* **46**, 1023 (2016).
- [43] B. R. Sutherland, U. Achatz, C.-c. P. Caulfield, and J. M. Klymak, Recent progress in modeling imbalance in the atmosphere and ocean, *Phys. Rev. Fluids* **4**, 010501 (2019).
- [44] E. Lindborg, The energy cascade in a strongly stratified fluid, *J. Fluid Mech.* **550**, 207 (2006).
- [45] J. J. Riley and E. Lindborg, Stratified turbulence: A possible interpretation of some geophysical turbulence measurements, *J. Atmos. Sci.* **65**, 2416 (2008).
- [46] L. G. Shapiro and G. C. Stockman, *Computer Vision* (Prentice Hall, New Jersey, 2001).
- [47] S. B. Pope, *Turbulent Flows* (Cambridge University Press, Cambridge, 2000).
- [48] D. K. Lilly, Stratified turbulence and the mesoscale variability of the atmosphere, *J. Atmos. Sci.* **40**, 749 (1983).
- [49] G. R. Spedding, F. K. Browand, and A. M. Fincham, The long-time evolution of the initially turbulent wake of a sphere in a stable stratification, *Dyn. Atmos. Oceans* **23**, 171 (1996).
- [50] O. Praud, A. M. Fincham, and J. Sommeria, Decaying grid turbulence in a strongly stratified fluid, *J. Fluid Mech.* **522**, 1 (2005).
- [51] A. M. Fincham, T. Maxworthy, and G. R. Spedding, Energy dissipation and vortex structure in freely decaying, stratified grid turbulence, *Dyn. Atmos. Oceans* **23**, 155 (1996).
- [52] J. J. Riley and S. M. de Bruyn Kops, Dynamics of turbulence strongly influenced by buoyancy, *Phys. Fluids* **15**, 2047 (2003).
- [53] D. A. Hebert and S. M. de Bruyn Kops, Relationship between vertical shear rate and kinetic energy dissipation rate in stably stratified flows, *Geophys. Res. Lett.* **33**, L06602 (2006).
- [54] S. M. de Bruyn Kops and J. J. Riley, The effects of stable stratification on the decay of initially isotropic homogeneous turbulence, *J. Fluid Mech.* **860**, 787 (2019).
- [55] H. Peters, M. C. Gregg, and J. M. Toole, On the parameterization of equatorial turbulence, *J. Geophys. Res.* **93**, 1199 (1988).
- [56] J. N. Moum, D. R. Caldwell, and C. A. Paulson, Mixing in the equatorial surface layer and thermocline, *J. Geophys. Res.* **94**, 2005 (1989).
- [57] W. D. Smyth, J. N. Moum, and D. R. Caldwell, The efficiency of mixing in turbulent patches: Inferences from direct simulations and microstructure observations, *J. Phys. Oceanogr.* **31**, 1969 (2001).
- [58] C. J. Howland, J. R. Taylor, and C. P. Caulfield, Shear-induced breaking of internal gravity waves, *J. Fluid Mech.* **921**, A24 (2021).
- [59] C. P. Caulfield, Layering, instabilities, and mixing in turbulent stratified flows, *Ann. Rev. Fluid Mech.* **53**, 113 (2021).
- [60] H. Salehipour, W. R. Peltier, C. B. Whalen, and J. A. MacKinnon, A new characterization of the turbulent diapycnal diffusivities of mass and momentum in the ocean, *Geophys. Res. Lett.* **43**, 3370 (2016).
- [61] J. R. Taylor and Q. Zhou, A multi-parameter criterion for layer formation in a stratified shear flow using sorted buoyancy coordinates, *J. Fluid Mech.* **823**, R5 (2017).
- [62] O. M. Phillips, Turbulence in a strongly stratified fluid—Is it unstable? *Deep-Sea Res.* **19**, 79 (1972).
- [63] E. S. Posmentier, The generation of salinity finestructure by vertical diffusion, *J. Phys. Oceanogr.* **7**, 298 (1977).